

Safe Multi-Robotic Arm Interaction via 3D Convex Shapes

Ali Umut Kaypak, Shiqing Wei, Prashanth Krishnamurthy, Farshad Khorrami

Abstract—Inter-robot collisions pose a significant safety risk when multiple robotic arms operate in close proximity. We present an online collision avoidance methodology leveraging 3D convex shape-based High-Order Control Barrier Functions (HOCBFs) to address this issue. While prior works focused on using Control Barrier Functions (CBFs) for human-robotic arm and single-arm collision avoidance, we explore the problem of collision avoidance between multiple robotic arms operating in a shared space. In our methodology, we utilize the proposed HOCBFs as centralized and decentralized safety filters. These safety filters are compatible with any nominal controller and ensure safety without significantly restricting the robots' workspace. A key challenge in implementing these filters is the computational overhead caused by the large number of safety constraints and the computation of a Hessian matrix per constraint. We address this challenge by employing numerical differentiation methods to approximate computationally intensive terms. The effectiveness of our method is demonstrated through extensive simulation studies and real-world experiments with Franka Research 3 robotic arms.

I. INTRODUCTION

The deployment of robots in unstructured dynamic environments necessitates effective collision prevention mechanisms. Various approaches have been proposed for this purpose, including Model Predictive Control (MPC)-based safety strategies [1], [2] and CBF-based methods [3]–[8]. CBF-based methods have received attention because of their ability to enforce forward invariance of safety sets while maintaining computational efficiency in many scenarios. Leveraging these properties, recent research has extensively explored their application in inter-robot collision avoidance, particularly for safe navigation in mobile robot systems [4]–[7]. However, despite the importance of multi-robotic arm interaction in specific applications [9], [10], CBF-based safety certificates for ensuring safe multi-robotic arm interaction remain largely unexplored. This work addresses this gap by investigating the application of CBFs that enhance safety during multi-robotic arm interactions and collaborative tasks.

CBFs are often used as constraints in Quadratic Programming (QP) to enforce safety [11]. The QP aims to keep the control input as close to the nominal controller as possible while obeying the safety constraints. To generalize this framework for systems whose relative degree with respect

to the constraint function is higher than one, HOCBFs were introduced [12], [13]. Our methodology is built on this concept by employing HOCBFs for collision avoidance among 3D convex shapes, as introduced in [3]. We extend the use of HOCBFs from single robotic arm collision avoidance to inter-robotic arm collision avoidance by utilizing them in pairwise robotic arm dynamics.

The key challenge in utilizing 3D Convex Shape-based HOCBFs in multi-robotic arms, compared to a single arm, is the increased computational overhead. This arises from calculating more constraints at every sampling time. Additionally, in multi-robot settings, all the 3D convex shapes used in the HOCBFs are dynamic. This further intensifies the computational burden. We address this issue by approximating computationally intensive terms via numerical derivative filters. Our contributions in this paper are summarized as follows: (1) Developing HOCBFs that ensure robot safety in multi-robotic arm settings and utilizing them in centralized and decentralized paradigms; (2) addressing the computational challenges of deploying these HOCBFs by estimating the computationally intensive terms with numerical derivative filters; and (3) validating the proposed method through extensive simulations and real-world experiments.

II. RELATED WORKS

CBFs in Inter-Robot Collision Avoidance: The use of CBFs to prevent collisions in multi-robot systems is an active research area, with various methodologies proposed for different scenarios [4]–[8]. For instance, centralized and decentralized CBF-based safety filters for planar mobile robots were introduced in [4]. A CBF-based methodology was developed for the safe control of drone swarms in [6], [14]. In addition, a distributed controller for the safe navigation of mobile robots was proposed in [8]. Similarly, HOCBFs were employed to generate safety-assured trajectories for multiple legged robots in [5]. However, extending these approaches to the multi-robotic arm setting is not straightforward. Although some work [15], [16] applied CBFs to ensure safe human-multiple robot hand interaction, they did not address possible collisions between robot bodies. This is the first work applying CBFs for collision avoidance among multiple robotic arms.

Inter-Robotic Arm Collision Avoidance: Collision handling between robotic arms can be categorized into online [17]–[19] and offline [20], [21] methods. Offline methods predefine commands and trajectories, while online methods address collisions in real time. Various online strategies have been explored. For example, collision maps were utilized to detect potential collisions and adjust command execution

The authors are with Control/Robotics Research Laboratory, Electrical and Computer Engineering Department, Tandon School of Engineering, New York University, Brooklyn, NY 11201, USA. E-mail: {ak10531, shiqing.wei, prashanth.krishnamurthy, khorrami}@nyu.edu.

This work was supported in part by the Army Research Office under grant numbers W911NF-21-1-0155 and W911NF-22-1-0028 and New York University Abu Dhabi (NYUAD) Center for Artificial Intelligence and Robotics (CAIR), funded by Tamkeen under the NYUAD Research Institute Award CG010.

times while preserving the path in [18]. Nonlinear MPC was employed for online trajectory planning, incorporating collision avoidance into the optimization constraints in [19]. Additionally, a motion planning method based on Soft Actor-Critic was proposed in [17] to prevent collisions in dual-robotic arms. In contrast to these approaches, we introduce a CBF-based method that can be seamlessly integrated as a filtering layer with any nominal controller.

III. NOTATIONS

The set of real numbers and the set of natural numbers are denoted by \mathbb{R} and \mathbb{N} , respectively. \mathbb{R}^n and $\mathbb{R}^{m \times n}$ represent real-valued n -dimensional column vectors and real-valued m -by- n matrices, respectively. The n -by- n identity matrix is denoted by \mathbf{I}_n . A function is \mathcal{C}^k if it is k -times differentiable with a continuous k th derivative. A continuous function $\Gamma : [0, a) \rightarrow [0, \infty)$, $a > 0$ is a class \mathcal{K} function if it is strictly increasing and $\Gamma(0) = 0$. For a \mathcal{C}^2 scalar function $h : \mathbb{R}^n \rightarrow \mathbb{R}$, $\nabla_{\mathbf{x}} h \in \mathbb{R}^k$ represents the gradient of h with respect to the vector $\mathbf{x} \in \mathbb{R}^k$, $k \leq n$, and $\nabla_{\mathbf{x}}^2 h \in \mathbb{R}^{k \times k}$ represents the Hessian of the function with respect to the vector \mathbf{x} . For a vector-valued \mathcal{C}^1 function $f : \mathbb{R}^q \rightarrow \mathbb{R}^m$, $\frac{\partial f}{\partial \mathbf{x}}$ represents the partial derivative of f , and it is an m -by- k matrix, where $\mathbf{x} \in \mathbb{R}^k$ and $k \leq q$. $L_f h(\mathbf{x})$ stands for the Lie derivative of a scalar function h with respect to a vector field f with $m = n$. The boundary of a set A is represented by ∂A . For a column vector $\mathbf{x} \in \mathbb{R}^n$ and a row vector $\mathbf{y} \in \mathbb{R}^{1 \times n}$, $\mathbf{x}_{[k]}$ and $\mathbf{y}_{[k]}$ denote the k th element of the vectors \mathbf{x} and \mathbf{y} , respectively. Similarly, $\mathbf{x}_{[k:l]}$ and $\mathbf{y}_{[k:l]}$, where $k < l \leq n$, represent the subvector $[\mathbf{x}_{[k]} \ \dots \ \mathbf{x}_{[l]}]^T$ and the subvector $[\mathbf{y}_{[k]} \ \dots \ \mathbf{y}_{[l]}]$, respectively.

IV. BACKGROUND

A. High Order Control Barrier Functions

Consider an affine control system in the form

$$\dot{\mathbf{x}} = f(\mathbf{x}) + g(\mathbf{x})\mathbf{u}, \quad (1)$$

where $f : \mathbb{R}^n \rightarrow \mathbb{R}^n$ and $g : \mathbb{R}^n \rightarrow \mathbb{R}^{n \times q}$ are globally Lipschitz \mathcal{C}^1 functions with the state vector $\mathbf{x} \in \mathbb{R}^n$ and input vector $\mathbf{u} \in \mathcal{U} \subset \mathbb{R}^q$, where \mathcal{U} denotes a closed set of possible control input values (taking into account physical constraints). For a given \mathcal{C}^r function $h(\mathbf{x}) : \mathbb{R}^n \rightarrow \mathbb{R}$ and r class \mathcal{K} functions $\Gamma_k(\cdot)$, $k \in \{1, \dots, r\}$, a sequence of functions and their superlevel sets are defined as follows:

$$\begin{aligned} \psi_0(\mathbf{x}) &= h(\mathbf{x}), \\ \psi_k(\mathbf{x}) &= \left(\frac{d}{dt} + \Gamma_k \right) \psi_{k-1}(\mathbf{x}), \quad k \in \{1, \dots, r\}, \\ C_k &= \{\mathbf{x} : \psi_{k-1}(\mathbf{x}) \geq 0\}, \quad k \in \{1, \dots, r\}. \end{aligned} \quad (2)$$

Definition 1 (Time-invariant HOCBFs [13]). *Let C_k , $k \in \{1, \dots, r\}$ and $\psi_k(\mathbf{x})$, $k \in \{0, \dots, r\}$ be defined by (2). A function $h : \mathbb{R}^n \rightarrow \mathbb{R}$ is a time-invariant HOCBF of relative degree r for system (1) if there exist differentiable class \mathcal{K} functions Γ_k , $k \in \{1, \dots, r\}$ such that:*

$$\sup_{\mathbf{u} \in \mathcal{U}} [L_f \psi_{r-1}(\mathbf{x}) + L_g \psi_{r-1}(\mathbf{x})\mathbf{u} + \Gamma_r(\psi_{r-1}(\mathbf{x}))] \geq 0 \quad (3)$$

for all $\mathbf{x} \in C_1 \cap \dots \cap C_r$.

Since this paper uses time-invariant HOCBFs, we provide the definition specifically for the time-invariant case rather than the general formulation. Additionally, in Definition 1, we incorporate the ψ_{r-1} notation within the supremum operator, which is equivalent to

$$\begin{aligned} L_f^r h(\mathbf{x}) + L_g L_f^{r-1} h(\mathbf{x})\mathbf{u} + \sum_{i=1}^{r-1} L_f^i (\Gamma_{r-i} \circ \psi_{r-i-1})(\mathbf{x}) \\ + \Gamma_r(\psi_{r-1}(\mathbf{x})), \end{aligned} \quad (4)$$

as the relative degree of h with respect to system (1) is r .

Theorem 1 (Theorem 4 in [13] for time-invariant HOCBFs). *Given an HOCBF h from Definition 1, and with the associated sets C_k , $k \in \{1, \dots, r\}$ defined by (2), if $x(t_0) \in \mathcal{C} := C_1 \cap \dots \cap C_r$, then any Lipschitz continuous controller $\mathbf{u}(t) \in K_{\text{HOCBF}}(\mathbf{x}) := \{\mathbf{u} \in \mathcal{U} : L_f \psi_{r-1}(\mathbf{x}) + L_g \psi_{r-1}(\mathbf{x})\mathbf{u} + \Gamma(\psi_{r-1}(\mathbf{x})) \geq 0\} \forall t \geq t_0$ renders the set \mathcal{C} forward invariant for the system (1).*

B. Convex Shapes for Defining Safety in Robotic Arms

We utilize 3D convex shapes, specifically ellipsoids, to construct collision bodies encompassing the links and end effectors of robotic arms. We use scaling functions to represent these collision bodies as their 1-sublevel sets in \mathbb{R}^3 .

Definition 2 (Scaling functions [22]). *A class \mathcal{C}^2 function $\mathcal{F}_A : \mathbb{R}^{n_p} \times \mathbb{R}^{n_\theta} \rightarrow \mathbb{R}$ is called a scaling function (with parameters $\theta \in \mathbb{R}^{n_\theta}$) for a closed set $A \subset \mathbb{R}^{n_p}$ with non-empty interior if \mathcal{F}_A is convex in the first argument and*

$$A = \{\mathbf{p} \in \mathbb{R}^{n_p} \mid \mathcal{F}_A(\mathbf{p}, \theta) \leq 1\}. \quad (5)$$

For a given convex set $A \subset \mathbb{R}^{n_p}$, the parameter θ determines the position and the orientation of the set in \mathbb{R}^{n_p} , while the parameter \mathbf{p} is used to evaluate the function, satisfying $\mathcal{F}_A(\mathbf{p}, \theta) \leq 1$ for $\mathbf{p} \in A$. Consequently,

$$\mathbf{p} \in \partial A(\theta) \iff \mathcal{F}_A(\mathbf{p}, \theta) = 1. \quad (6)$$

Let A and B be convex sets in \mathbb{R}^{n_p} with $A \cap B = \emptyset$, and let their corresponding scaling functions be $\mathcal{F}_A(\mathbf{p}, \theta)$ and $\mathcal{F}_B(\mathbf{p}, \theta)$, respectively. In [3], determining the minimum level set of $\mathcal{F}_A(\mathbf{p}, \theta)$ that intersects B is formulated as the following optimization problem:

$$\begin{aligned} \alpha^*(\theta) &= \min_{\mathbf{p} \in \mathbb{R}^{n_p}} \mathcal{F}_A(\mathbf{p}, \theta) \\ \text{s.t. } &\mathcal{F}_B(\mathbf{p}, \theta) \leq 1. \end{aligned} \quad (7)$$

Although there are alternative formulations, we choose the approach in [3] because it facilitates the use of torque control in robotic arms. Let $\mathbf{p}^*(\theta)$ denote the optimal solution to this problem. The following theorem provides sufficient conditions for the differentiability order of $\alpha^*(\theta)$:

Theorem 2 (Theorem 2 in [3]). *Let \mathcal{F}_A and \mathcal{F}_B be scaling functions corresponding to the sets A and B , respectively, with $A \cap B = \emptyset$. Assume that one of \mathcal{F}_A and \mathcal{F}_B has a positive definite Hessian in \mathbf{p} . If the scaling functions \mathcal{F}_A*

and \mathcal{F}_B are C^{k+1} (with $k \geq 1$) in \mathbf{p} and $\boldsymbol{\theta}$, then α^* is C^k in $\boldsymbol{\theta}$.

Under the same assumptions, it was shown in [3] that

$$\nabla_{\boldsymbol{\theta}} \alpha^*(\boldsymbol{\theta}) = \left(\frac{\partial \mathbf{p}^*}{\partial \boldsymbol{\theta}}(\boldsymbol{\theta}) \right)^T \nabla_{\mathbf{p}} \mathcal{F}_A(\mathbf{p}^*, \boldsymbol{\theta}) + \nabla_{\boldsymbol{\theta}} \mathcal{F}_A(\mathbf{p}^*, \boldsymbol{\theta}). \quad (8)$$

V. SAFE MULTI-ROBOTIC ARM INTERACTION

In Sections V-A and V-B, we introduce HOCBFs for preventing inter-robot collisions and present their application in centralized and decentralized control paradigms, respectively.

A. Construction of HOCBFs for Multi-Robotic Arm Setting

Consider an environment with several robotic arms and each robotic arm in the environment is indexed by the set $\mathcal{I} \subset \mathbb{N}$. Dynamics of robotic arm $i \in \mathcal{I}$ are written as [23]:

$$M_i(\mathbf{q}_i) \ddot{\mathbf{q}}_i + \underbrace{C_i(\mathbf{q}_i, \dot{\mathbf{q}}_i) \dot{\mathbf{q}}_i + F_i(\dot{\mathbf{q}}_i) + g_i(\mathbf{q}_i)}_{\sigma_i(\mathbf{q}_i, \dot{\mathbf{q}}_i)} = \mathbf{u}_i \quad (9)$$

where $\mathbf{q}_i \in \mathbb{R}^{n_i}$ and $\mathbf{u}_i \in \mathbb{R}^{n_i}$ are the joint vector and actuator torque vector for robot i , respectively. $M_i(\mathbf{q}_i) \in \mathbb{R}^{n_i \times n_i}$ is the symmetric positive definite mass matrix, $C_i(\mathbf{q}_i, \dot{\mathbf{q}}_i) \in \mathbb{R}^{n_i \times n_i}$ consists of centrifugal and Coriolis terms, $F_i(\dot{\mathbf{q}}_i) \in \mathbb{R}^{n_i}$ is the friction vector, and $g_i(\mathbf{q}_i) \in \mathbb{R}^{n_i}$ is the gravity vector for robot i . By utilizing (9), the pairwise robot dynamics for two different robot i and j ($i \neq j$) can be expressed in a control affine system form as follows:

$$\underbrace{\frac{d}{dt} \begin{bmatrix} \mathbf{q}_i \\ \dot{\mathbf{q}}_i \\ \mathbf{q}_j \\ \dot{\mathbf{q}}_j \end{bmatrix}}_{\mathbf{x}_{ij}} = \underbrace{\begin{bmatrix} \dot{\mathbf{q}}_i \\ M_i^{-1}(\mathbf{q}_i) \sigma_i(\mathbf{q}_i, \dot{\mathbf{q}}_i) \\ \dot{\mathbf{q}}_j \\ M_j^{-1}(\mathbf{q}_j) \sigma_j(\mathbf{q}_j, \dot{\mathbf{q}}_j) \end{bmatrix}}_{f(\mathbf{x}_{ij})} + \underbrace{\begin{bmatrix} 0 & 0 \\ M_i^{-1}(\mathbf{q}_i) & 0 \\ 0 & 0 \\ 0 & M_j^{-1}(\mathbf{q}_j) \end{bmatrix}}_{g(\mathbf{x}_{ij})} \underbrace{\begin{bmatrix} \mathbf{u}_i \\ \mathbf{u}_j \end{bmatrix}}_{\mathbf{u}_{ij}}. \quad (10)$$

To construct a scaling function for a robot's link or end effector, we follow the construction recipe described in [3]. For a given $\mathbf{p}^W \in \mathbb{R}^3$ in the world frame, the point is first transformed into body frame coordinates as $\mathbf{p}^B = \mathbf{R}_W^B(\mathbf{p}^W - \mathbf{o}_B^W)$ where \mathbf{R}_W^B denotes the orientation of the world frame expressed in the body frame, and \mathbf{o}_B^W represents the origin of the body frame in the world frame.

An analytical solution for (7) is available when both scaling functions are ellipsoids [24]. In contrast, computing the HOCBF coefficients for other 3D convex shapes requires numerically solving (7) at every iteration. This process is computationally costly for real-time robot control. Therefore, we use ellipsoids to represent the robot links and end effector. The scaling functions used in the remainder of this paper are of the following form:

$$\mathcal{F}(\mathbf{p}^W) = (\mathbf{R}_W^B(\mathbf{p}^W - \mathbf{o}_B^W) - \boldsymbol{\mu})^T \mathbf{Q} (\mathbf{R}_W^B(\mathbf{p}^W - \mathbf{o}_B^W) - \boldsymbol{\mu}) \quad (11)$$

where $\boldsymbol{\mu} \in \mathbb{R}^3$ represents the ellipsoid center, and $\mathbf{Q} \in \mathbb{R}^{3 \times 3}$ is a positive definite and symmetric matrix that determines the ellipsoid's principal axes and scaling along each axis.

Consider two distinct robot arms, indexed by i and j ($i \neq j$), and let k and l denote a link or end effector of robots i and j , respectively. The link centers in the world frame and their quaternions are given by $\mathbf{o}_{i_k}, \mathbf{o}_{j_l} \in \mathbb{R}^3$ and $\boldsymbol{\xi}_{i_k}, \boldsymbol{\xi}_{j_l} \in \mathbb{R}^4$, respectively. Using these link centers and orientations, an ellipsoid scaling function is defined to represent each link.

Defining $\boldsymbol{\theta}_{i_k j_l} := [\mathbf{o}_{i_k}^T \ \boldsymbol{\xi}_{i_k}^T \ \mathbf{o}_{j_l}^T \ \boldsymbol{\xi}_{j_l}^T]^T \in \mathbb{R}^{14}$, we obtain the HOCBF and the ψ s in (2) as follows:

$$\begin{aligned} \psi_0^{i_k j_l}(\mathbf{x}_{ij}) &= h_{i_k j_l}(\mathbf{x}_{ij}) = \alpha^*(\boldsymbol{\theta}_{i_k j_l}) - \alpha_0, \quad \alpha_0 > 0 \\ \psi_w^{i_k j_l}(\mathbf{x}_{ij}) &= \left(\frac{d}{dt} + \Gamma_w \right) \psi_{w-1}^{i_k j_l}(\mathbf{x}_{ij}), \quad w \in \{1, 2\}. \end{aligned} \quad (12)$$

By applying the chain rule, the time derivative of $h_{i_k j_l}(\mathbf{x}_{ij})$ is given by

$$\dot{h}_{i_k j_l}(\mathbf{x}_{ij}) = (\nabla_{\boldsymbol{\theta}} \alpha^*(\boldsymbol{\theta}_{i_k j_l}))^T \dot{\boldsymbol{\theta}}_{i_k j_l} \quad (13)$$

where

$$\dot{\boldsymbol{\theta}}_{i_k j_l} = \mathbf{T}_{ij}^{kl} \boldsymbol{\Omega}_{ij}^{kl} \dot{\mathbf{q}}_{ij} \quad (14)$$

with

$$\begin{aligned} \mathbf{T}_{ij}^{kl} &= \begin{bmatrix} \mathbf{I}_{3 \times 3} & 0 & 0 & 0 \\ 0 & 0.5Q(\boldsymbol{\xi}_{i_k}) & 0 & 0 \\ 0 & 0 & \mathbf{I}_{3 \times 3} & 0 \\ 0 & 0 & 0 & 0.5Q(\boldsymbol{\xi}_{j_l}) \end{bmatrix}, \\ \boldsymbol{\Omega}_{ij}^{kl} &= \begin{bmatrix} J_{i_k}(\mathbf{q}_i) & 0 \\ 0 & J_{j_l}(\mathbf{q}_j) \end{bmatrix}, \quad \dot{\mathbf{q}}_{ij} = \begin{bmatrix} \dot{\mathbf{q}}_i \\ \dot{\mathbf{q}}_j \end{bmatrix}. \end{aligned} \quad (15)$$

with the matrix $Q(\boldsymbol{\xi})$ defined as

$$Q(\boldsymbol{\xi}) = \begin{bmatrix} \xi_w & \xi_z & -\xi_y \\ -\xi_z & \xi_w & \xi_x \\ \xi_y & -\xi_x & \xi_w \\ -\xi_x & -\xi_y & -\xi_z \end{bmatrix}, \quad (16)$$

and $J_{i_k}(\mathbf{q}_i) \in \mathbb{R}^{6 \times n_i}$ and $J_{j_l}(\mathbf{q}_j) \in \mathbb{R}^{6 \times n_j}$ are the geometric Jacobian matrices for the link k in robot i and l in robot j .

Utilizing (12) and (13), along with the chain rule, we obtain $L_g \psi_1^{i_k j_l}(\mathbf{x}_{ij})$ and $L_f \psi_1^{i_k j_l}(\mathbf{x}_{ij})$ as follows:

$$L_g \psi_1^{i_k j_l}(\mathbf{x}_{ij}) = (\nabla_{\boldsymbol{\theta}} \alpha^*(\boldsymbol{\theta}_{i_k j_l}))^T \mathbf{T}_{ij}^{kl} \boldsymbol{\Omega}_{ij}^{kl} \boldsymbol{\Upsilon}_{ij}, \quad (17)$$

$$\begin{aligned} L_f \psi_1^{i_k j_l}(\mathbf{x}_{ij}) &= \dot{\boldsymbol{\theta}}_{i_k j_l}^T (\nabla_{\boldsymbol{\theta}}^2 \alpha^*(\boldsymbol{\theta}_{i_k j_l})) \dot{\boldsymbol{\theta}}_{i_k j_l} + \dot{\Gamma}_1(\psi_0^{i_k j_l}(\mathbf{x}_{ij})) \\ &+ (\nabla_{\boldsymbol{\theta}} \alpha^*(\boldsymbol{\theta}_{i_k j_l}))^T \left(\dot{\mathbf{T}}_{ij}^{kl} \boldsymbol{\Omega}_{ij}^{kl} \dot{\mathbf{q}}_{ij} + \mathbf{T}_{ij}^{kl} \dot{\boldsymbol{\Omega}}_{ij}^{kl} \dot{\mathbf{q}}_{ij} + \boldsymbol{\Upsilon}_{ij} \sigma_{ij} \right), \end{aligned} \quad (18)$$

where

$$\boldsymbol{\Upsilon}_{ij} = \begin{bmatrix} M_i^{-1}(\mathbf{q}_i) & 0 \\ 0 & M_j^{-1}(\mathbf{q}_j) \end{bmatrix}, \quad \sigma_{ij} = \begin{bmatrix} \sigma_i(\mathbf{q}_i, \dot{\mathbf{q}}_i) \\ \sigma_j(\mathbf{q}_j, \dot{\mathbf{q}}_j) \end{bmatrix}. \quad (19)$$

$L_g \psi_1^{i_k j_l}(\mathbf{x}_{ij})$ and $L_f \psi_1^{i_k j_l}(\mathbf{x}_{ij})$ can be computed analytically using sensor data, robot kinematics, and robot dynamics.

B. Centralized-Decentralized HOCBF Filters

The centralized HOCBF filter employs a single shared filter to process all robots' nominal input signals collectively, whereas the decentralized filter applies individual safety filters to each robot in the environment. The notion of multi-robot safety in this paper is formally defined below.

Definition 3. Consider an environment with multiple robotic arms indexed by the set $\mathcal{I} \subseteq \mathbb{N}$, with their dynamics given by (9). For each robot $i \in \mathcal{I}$, let $\mathcal{P}_i \subseteq \mathbb{N}$ index the links and end-effector of robot i . For all $i, j \in \mathcal{I}$ with $i \neq j$, and for all $k \in \mathcal{P}_i$ and $l \in \mathcal{P}_j$, define the sets:

$$C_w^{i_k j_l} := \{\mathbf{x}_{ij} : \psi_{w-1}^{i_k j_l}(\mathbf{x}_{ij}) \geq 0\}, \quad w \in \{1, 2\} \quad (20)$$

where $\psi_w^{i_k j_l}(\mathbf{x}_{ij})$ is defined as in (12). The multi-robot system is *safe* if, for all $i, j \in \mathcal{I}$ with $i \neq j$, and for all $k \in \mathcal{P}_i$ and $l \in \mathcal{P}_j$, we have $\mathbf{x}_{ij}(t) \in C_1^{i_k j_l} \forall t \geq t_0$ whenever $\mathbf{x}_{ij}(t_0) \in C_1^{i_k j_l}$.

In the centralized safety filter, a single QP determines each robot's control input, i.e. \mathbf{u}_i , ensuring compliance with the safety constraints in Definition 3. Let $\mathbf{u}_{\text{nom}_i}$ denote the nominal control for robot $i \in \mathcal{I}$. Define the stacked nominal control input and the stacked control input as $\mathbf{u}_{\text{nom}} := [\mathbf{u}_{\text{nom}_i}^T \mid i \in \mathcal{I}]^T$, $\mathbf{u} := [\mathbf{u}_i^T \mid i \in \mathcal{I}]^T$, respectively. Given a positive definite matrix \mathbf{P} , the *centralized-HOCBF-QP* is formulated as:

$$\begin{aligned} \min_{\mathbf{u}_i \in \mathcal{U}_i} \quad & (\mathbf{u} - \mathbf{u}_{\text{nom}})^T \mathbf{P} (\mathbf{u} - \mathbf{u}_{\text{nom}}) \\ \text{s.t.} \quad & \forall i, j \in \mathcal{I}, \text{ with } i \neq j, \forall k \in \mathcal{P}_i \text{ and } \forall l \in \mathcal{P}_j \\ & L_g \psi_1^{i_k j_l}(\mathbf{x}_{ij}) \mathbf{u}_{ij} \geq -L_f \psi_1^{i_k j_l}(\mathbf{x}_{ij}) - \Gamma_2(\psi_1^{i_k j_l}(\mathbf{x}_{ij})). \end{aligned} \quad (21)$$

The solution to this optimization problem is unstacked in the same order as \mathbf{u}_{nom} and provided to the respective robots in the environment. By Theorem 1, if the multi-robot system starts in a configuration where

$$\mathbf{x}_{ij}(t_0) \in \bigcap_{\substack{w=1,2 \\ k \in \mathcal{P}_i, l \in \mathcal{P}_j}} C_w^{i_k j_l}, \quad \forall i, j \in \mathcal{I}, i \neq j \quad (22)$$

and (21) is feasible, then the proposed filter ensures safety for all $t \geq t_0$. A typical place where (21) may become infeasible is in highly cluttered environments where a robot's movement is prevented by multiple surrounding robots. Such a scenario represents a geometrical constraint/infeasibility in the environment. When there is no priority among robot tasks, the matrix \mathbf{P} in *centralized-HOCBF-QP* is chosen as the identity matrix, reducing the cost function to $\|\mathbf{u} - \mathbf{u}_{\text{nom}}\|_2^2$. To introduce task priorities, a diagonal matrix with distinct positive weights is used for each robot's control signal, thereby capturing each robot's relative responsibility for maintaining overall safety.

The computational cost of solving the QP problem increases with the number of optimization parameters, which grows as the number of robots increases. Therefore, *centralized-HOCBF-QP* faces scalability challenges due to

the computational burden of solving a large-scale optimization problem for real-time control. *Decentralized-HOCBF-QP* provides a viable solution for this problem by enabling each robot to independently filter its own nominal control input in parallel during task execution, at the cost of suboptimal solutions. For robot $i \in \mathcal{I}$, *decentralized-HOCBF-QP* is formulated as:

$$\begin{aligned} \min_{\mathbf{u}_i \in \mathcal{U}} \quad & \|\mathbf{u}_i - \mathbf{u}_{\text{nom}_i}\|_2^2 \\ \text{s.t.} \quad & \forall j \in \mathcal{I}, \text{ with } i \neq j, \forall k \in \mathcal{P}_i \text{ and } \forall l \in \mathcal{P}_j \\ & L_g \psi_1^{i_k j_l}(\mathbf{x}_{ij})_{[1:n_i]} \mathbf{u}_i \geq -c_{ij} (L_f \psi_1^{i_k j_l}(\mathbf{x}_{ij}) \\ & \quad + \Gamma_2(\psi_1^{i_k j_l}(\mathbf{x}_{ij}))). \end{aligned} \quad (23)$$

In decentralized filtering, priority among different robot tasks is not introduced through the cost function, as it includes only a single robot's control. Instead, it is established via the scalar c_{ij} , which appears in the QP constraints. The scalar satisfies $0 \leq c_{ij} = 1 - c_{ji} \leq 1$ and represents the responsibility of robot i in the HOCBF constraints shared with robot j . Assuming each robot has access to other robots' states, the coefficients of the inequality constraints can either be computed independently by each robot or computed collectively and shared. The choice between these approaches depends on the specific multi-robot system setting.

As with *centralized-HOCBF-QP*, Theorem 1 guarantees that if the multi-robot system starts in a configuration where condition (22) holds and (23) is feasible for all $i \in \mathcal{I}$ at all times, then *decentralized-HOCBF-QP* ensures safety for all $t \geq t_0$. However, the solution to *decentralized-HOCBF-QP* is suboptimal compared to the *centralized-HOCBF-QP* solution due to the hard task priorities imposed through the parameters c_{ij} in (23). This also reduces the feasibility set of the control inputs, which may render (23) infeasible for some $i \in \mathcal{I}$. To mitigate this issue, a relaxation method was introduced in decentralized QPs in prior work [4] for first-order CBFs. Following this approach, we propose *decentralized-HOCBF-relaxed-QP* and establish its theoretical foundation for HOCBFs in Theorem 3.

Theorem 3. Let h be a time-invariant HOCBF, and consider ψ_{k-1} with the corresponding safety sets \mathcal{C}_k for $k \in \{1, \dots, r\}$ as defined in (2). Suppose that the class \mathcal{K} functions Γ_k s used to define ψ_k s are locally Lipschitz. Furthermore, let $\phi(t)$ be continuous and satisfy $\phi(t) \geq 1$ for all $t \geq t_0$. Then, any locally Lipschitz continuous controller $\mathbf{u} : \mathbb{R}^n \rightarrow \mathbb{R}^q$ such that $\mathbf{u}(\mathbf{x}) \in K_{RHOCBF}(\mathbf{x}) := \{\mathbf{u} \in \mathcal{U} : L_f \psi_{r-1}(\mathbf{x}) + L_g \psi_{r-1}(\mathbf{x}) \mathbf{u} + \phi(t) \Gamma_r(\psi_{r-1}(\mathbf{x})) \geq 0\}$ will render the set $\mathcal{C} := \bigcap_{k=1}^r \mathcal{C}_k$ forward invariant for the system (1).

Proof. The proof is adapted along the lines of Theorem V.1 in [4]. First, consider the system $\dot{z} = -\Gamma_r(z)$ where Γ_r is a class \mathcal{K} function. The solution of the system is $z(t) = \sigma(z(0), t)$, where $\sigma(k, s)$ is a class \mathcal{KL} function and $\frac{\partial}{\partial s} \sigma(k, s) = -\Gamma_r(\sigma(k, s))$ [25]. Then the solution of the

relaxed system, i.e. $\dot{\hat{z}} = -\phi(t)\Gamma_r(\hat{z})$, is found as

$$\hat{z}(t) = \sigma \left(\hat{z}(0), \int_0^t \phi(\tau) d\tau \right). \quad (24)$$

The solution can be verified by

$$\begin{aligned} \frac{d \left(\sigma \left(\hat{z}(0), \int_0^t \phi(\tau) d\tau \right) \right)}{dt} &= \frac{\partial \sigma(\hat{z}(0), s)}{\partial s} \frac{d \left(\int_0^t \phi(\tau) d\tau \right)}{dt} \\ &= -\Gamma_r \left(\sigma \left(\hat{z}(0), \int_0^t \phi(\tau) d\tau \right) \right) \phi(t) = -\Gamma_r(\hat{z}) \phi(t) = \dot{\hat{z}} \end{aligned} \quad (25)$$

and

$$\sigma \left(\hat{z}(0), \int_0^0 \phi(\tau) d\tau \right) = \sigma(\hat{z}(0), 0) = \hat{z}(0). \quad (26)$$

The solution is unique because Γ_r is locally Lipschitz and ϕ is continuous. Since $\mathbf{u}(\mathbf{x}) \in K_{\text{RHOCBF}}(\mathbf{x})$, we have $\psi_{r-1}(\mathbf{x}) = L_f \psi_{r-1}(\mathbf{x}) + L_g \psi_{r-1}(\mathbf{x}) \mathbf{u} \geq -\phi(t)\Gamma_r(\psi_{r-1}(\mathbf{x}))$. From (24) and Comparison Lemma [25], it follows that

$$\psi_{r-1}(\mathbf{x}) \geq \sigma \left(\psi_{r-1}(\mathbf{x}(0)), \int_0^t \phi(\tau) d\tau \right). \quad (27)$$

Assuming $\mathbf{x}(0) \in \mathcal{C}$, the definition of \mathcal{C} implies $\psi_k(\mathbf{x}(0)) \geq 0$, $0 \leq k \leq r-1$. Since $\phi(t) \geq 1$, $\int_0^t \phi(\tau) d\tau$ is monotonically increasing with t and $\int_0^t \phi(\tau) d\tau \rightarrow \infty$ as $t \rightarrow \infty$. By the properties of \mathcal{KL} functions, for a fixed $u \geq 0$, $\sigma(u, v) \rightarrow 0$ as $v \rightarrow \infty$ and as it is decreasing, $\psi_{r-1}(\mathbf{x}) \geq 0$ for all $t \geq 0$. Given the recursive definition $\psi_k(\mathbf{x}) = \left(\frac{d}{dt} + \Gamma_k \right) \psi_{k-1}(\mathbf{x})$, if $\psi_k(\mathbf{x}) \geq 0$, then $\dot{\psi}_{k-1}(\mathbf{x}) \geq -\Gamma_k(\psi_{k-1}(\mathbf{x}))$. Since Γ_k is a class \mathcal{K} function and $\mathbf{x}(0) \in \mathcal{C}$, it follows by induction that $\psi_k(\mathbf{x}) \geq 0$ for $0 \leq k \leq r-1$. This establishes that $K_{\text{RHOCBF}}(\mathbf{x})$ renders the set forward-invariant for system (1). \square

As the only constraint on $\phi(t)$ is that it must be continuous, we follow [4] and introduce it as an optimization parameter in the decentralized QPs. The optimization problem includes the hyperparameter λ , which controls the trade-off between increasing $\phi(t)$ and adhering to the original objective, and is formulated for robot $i \in \mathcal{I}$ as follows:

$$\begin{aligned} \min_{\mathbf{u}_i \in \mathcal{U}, \phi_{i_k j_l} \geq 1} \quad & \|\mathbf{u}_i - \mathbf{u}_{\text{nom}i}\|_2^2 + \lambda \sum_{\substack{j \in \mathcal{I}, j \neq i \\ k \in \mathcal{P}_i, l \in \mathcal{P}_j}} (\phi_{i_k j_l} - 1)^2 \\ \text{s.t.} \quad & \forall j \in \mathcal{I}, \text{ with } i \neq j, \forall k \in \mathcal{P}_i \text{ and } \forall l \in \mathcal{P}_j, \\ & L_g \psi_1^{i_k j_l}(\mathbf{x}_{ij})_{[1:n_i]} \mathbf{u}_i \geq -c_{ij} L_f \psi_1^{i_k j_l}(\mathbf{x}_{ij}) \\ & \quad - c_{ij} \phi_{i_k j_l} \Gamma_2(\psi_1^{i_k j_l}(\mathbf{x}_{ij})). \end{aligned} \quad (28)$$

Theorem 3 guarantees that if the multi-robot system begins in a configuration satisfying condition (22) and (28) remains feasible for all $i \in \mathcal{I}$ at all times, then the *decentralized-HOCBF-relaxed-QP* maintains safety for all $t \geq t_0$.

VI. COMPUTATIONAL CHALLENGES IN COMPUTING HOCBFs FOR MULTI-ROBOTIC HAND SAFETY

In this section, we address the computational challenges of employing the HOCBFs in multi-robot environments.

During the experiments presented in Section VII, we observed that the primary computational overhead in HOCBF computations arises from computing $L_f \psi_1^{i_k j_l}(\mathbf{x}_{ij})$. While this overhead does not hinder computation of HOCBFs that prevent a single robot from colliding with static or dynamic obstacles as in [3], it poses significant computational challenges in multi-robot environments due to the large number of HOCBFs required to ensure multi-robot safety. For instance, while 14 HOCBFs are sufficient to protect the 7 links of a robotic arm from two obstacles, 48 HOCBFs are required to protect the last 4 links of the three robotic arms from colliding with each other. Furthermore, the need to define θ as a 14-dimensional vector for two moving objects—compared to 7 dimensions for a moving robot and a static obstacle—further amplifies the computational burden of HOCBF computations.

$L_f \psi_1^{i_k j_l}(\mathbf{x}_{ij})$ is computed as in (18). The primary bottleneck in this computation stems from calculating the Hessian $\nabla_{\theta}^2 \alpha^*(\theta_{i_k j_l}) \in \mathbb{R}^{14 \times 14}$. To reduce the computational cost, we introduce an alternative numerical approach to estimate the term $(\nabla_{\theta}^2 \alpha^*(\theta_{i_k j_l})) \dot{\theta}_{i_k j_l} = \frac{d}{dt} (\nabla_{\theta} \alpha^*(\theta_{i_k j_l}))$. We estimate this product instead of estimating the Hessian itself because estimating $\nabla_{\theta}^2 \alpha^*(\theta_{i_k j_l})$ is significantly more challenging. While approximating the time derivative of the gradient requires estimating only one partial derivative per element in $\nabla_{\theta} \alpha^*(\theta_{i_k j_l})$, estimating the full Hessian involves computing 14 distinct partial derivatives for each element.

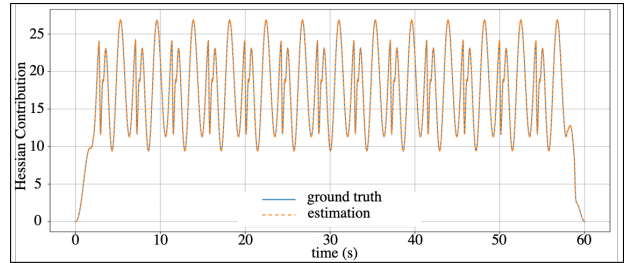


Fig. 1. An example of *Hessian contribution* estimation using backward difference approximation in an unnoisy MuJoCo Environment. The RMSE between the ground truth and the prediction is 0.01864.

We refer to the term $\dot{\theta}_{i_k j_l}^T (\nabla_{\theta}^2 \alpha^*(\theta_{i_k j_l})) \dot{\theta}_{i_k j_l}$ in (18) as *Hessian contribution* throughout the remainder of the paper. A straightforward way to approximate this term is to estimate each element of the time derivative of the gradient, i.e., $\frac{d}{dt} (\nabla_{\theta} \alpha^*(\theta_{i_k j_l}))_{[w]}$, using a backward difference approximation based on the current gradient and the one computed in the previous control loop. An example of *Hessian contribution* obtained using this method in a MuJoCo simulation [26], followed by a z-score-based outlier detection to mitigate numerical instabilities in the estimation, is shown in Fig. 1. As demonstrated in the figure, even this simple method provides an accurate estimation of the *Hessian contribution*, eliminating the need for explicit Hessian computation in the simulation environment. However, the backward difference approximation performs poorly in noisy data. Since real-robot sensor readings may be noisy and susceptible to environmental perturbations, this method

can lead to inaccurate estimations in real-robot scenarios. To overcome this issue, we use the Savitzky-Golay filter [27] in our methodology, where its parameters can be tuned according to the noise level.

Figure 2 demonstrates two examples of the *Hessian contribution* estimated using the Savitzky-Golay filter alongside their ground truth in an environment with two Franka Research 3 robotic arms. As shown in this figure and supported by the RMSE between the analytically computed and estimated *Hessian contribution*, we conclude that the proposed method achieves sufficient accuracy for estimating the *Hessian contribution* in a real robot environment. Additional evidence for the method’s accuracy is presented in Section VII, where the numerical estimation of the *Hessian contribution* does not compromise the safety of the robots.

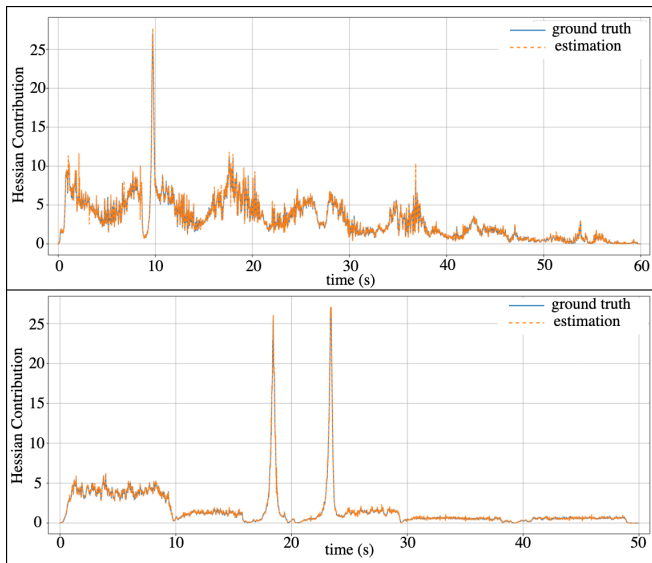


Fig. 2. **Two different examples of *Hessian contribution* estimation utilizing Savitzky-Golay filter in a real multi-robot environment.** The data and ground truth signals were collected from real experiments that use analytically computed *Hessian contributions*. The estimation was performed offline, simulating an online setting. The window length and polynomial order in the filter are set to 5 and 2, respectively. RMSE: 0.31149 (upper image) and 0.15137 (lower image).

A comparison of the time required to compute HOCBFs using the analytical and numerical methods is provided in Tab. I. The computations were performed on a computing system equipped with a 24-core Intel i7-13700KF processor and 32 GB of RAM. Parallel computing was utilized, with each HOCBF computation assigned to a separate thread for simultaneous execution. Due to the parallel computing, a linear increase in computation time with the number of HOCBFs is not observed in Tab. I. While the HOCBF computations, excluding the Savitzky-Golay filtering, were implemented in C++ using the `xtensor` library¹, the simulations were conducted in Python, employing the `scipy`² implementation of the Savitzky-Golay filter. The average in the table was computed over 3600 runs.

¹<https://xtensor.readthedocs.io>

²<https://scipy.org>

As shown in Tab. I, the proposed method for estimating *Hessian contribution* significantly reduces computational time. The proposed *Hessian contribution* estimation methodology enables scalability of HOCBFs described in Section V to scenarios involving more than two robotic arms and facilitates higher precision control for two-robot arm setups at sufficiently high update rates.

TABLE I
AVERAGE TIME (IN MILLISECONDS) REQUIRED TO COMPUTE HOCBFs USING THE ANALYTICALLY COMPUTED HESSIAN CONTRIBUTION AND THE SAVITZKY-GOLAY FILTER ESTIMATION.

# of HOCBFs	Analytical Method	Savitzky-Golay Filter Estimation
1	4.40	1.24
8	4.46	1.27
32	10.43	2.96
64	17.31	4.99
128	30.38	8.90
256	56.23	16.48

VII. EXPERIMENTS

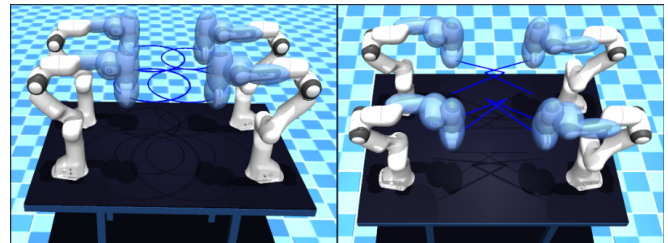


Fig. 3. **Trajectory following examples in the MuJoCo environment.** Ellipses covering the robot parts represent the 3D shapes used to define HOCBFs. Dark blue line segments in front of the end-effectors illustrate examples of intersecting trajectories.

We designed both simulation and real-robot experiments to evaluate the proposed method. In real-robot experiments, we demonstrated the applicability of the methodology under real-world conditions and showed the effect of utilizing numerical derivation in *Hessian-contribution* on the control update rate, while in simulations, we showcased its scalability to scenarios involving more than two robots and various path-following tasks. Additionally, we exhaustively compared centralized, decentralized, and relaxed-decentralized HOCBF filters in the simulations. In all experiments, joint accelerations were used as intermediate control input, with HOCBFs applied to them. These accelerations were subsequently converted into joint torques using the robot dynamics described in (9). Furthermore, equal responsibility was assigned to all robots for satisfying the HOCBF constraints by using an identity matrix for \mathbf{P} in (21) and setting $c_{ij} = 0.5$ in (23) and (28). λ in (28) was set to 10. We utilized OSQP [28] to solve the QP problems. For the nominal controller, we incorporated an inverse dynamics controller as the primary objective for trajectory-following in the operational space [23].

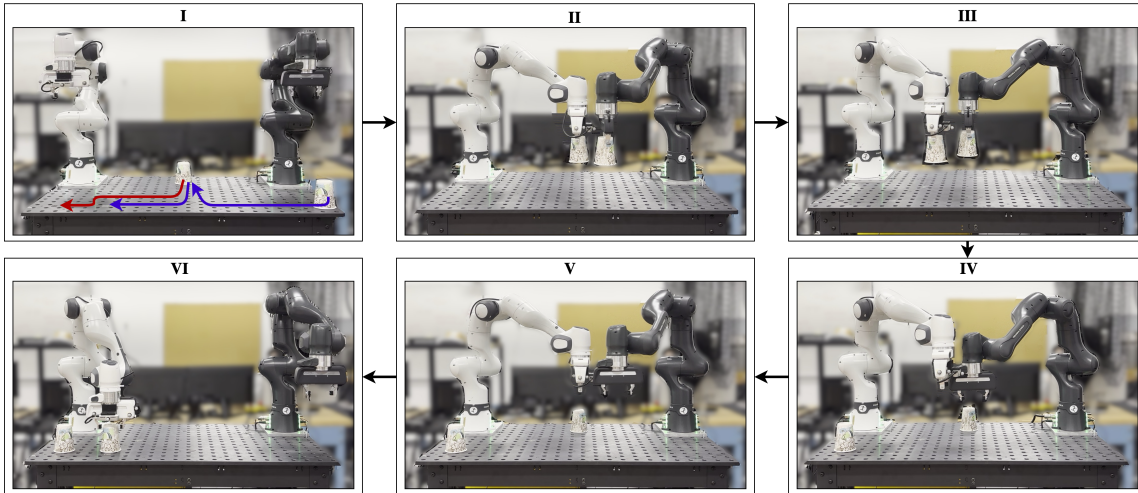


Fig. 4. **Two-robot pick-and-place example:** The white arm moves an object to its final position while the gray arm places another object in the first object’s initial spot, which the white arm later relocates. Their trajectories intersect twice (Images II and IV), but collisions are prevented by our method.

In the experiments, we utilized linear class \mathcal{K} functions for HOCBFs, i.e. $\Gamma_w(\psi_w^{i_k j_l}(\mathbf{x}_{ij})) = \Gamma_w \psi_w^{i_k j_l}(\mathbf{x}_{ij})$ in (12). We set $\Gamma_1 = 15$ and $\Gamma_2 = 15$ for these functions and selected $\alpha_0 = 1.03$ as the parameter in (12). In addition to the multi-robot safety HOCBFs, we incorporated angle, velocity, and torque constraints for each robot in all QPs to ensure the resulting controllers adhered to the robots’ physical limits.

A. Simulation Studies

We conducted our simulation experiments in MuJoCo [26]. The simulation environment, consisting of four Franka Research 3 robotic arms with intersecting workspaces, is illustrated in Fig. 3. Each robot’s end effector and last three links were enclosed by four ellipsoids to define HOCBFs, resulting in a total of 96 HOCBFs for multi-robot safety. In the simulation, we assumed that HOCBF calculations were performed in real-time, ensuring no control delays.

To simulate noise in robot sensors, we added Gaussian noise ($\mathcal{N}(0, 2.5 \times 10^{-3})$) into joint angles (rad) and joint angular velocities (rad/s). This noise also affected derived entities such as ellipsoid frame positions, orientations, and Jacobians. Due to operating system interruptions and CBF calculations potentially causing variations in the control update rate during real robot experiments, and since the Savitzky-Golay filter assumes a constant sampling rate, we scaled its sampling period hyperparameter with uniform noise, i.e., $\tilde{dt} = kdt$, where $k \sim \mathcal{U}(0.9, 1.1)$ and dt is the sampling time. The filter’s window length and polynomial order were set to 25 and 2, respectively. We conducted 40 experiments for each filter with diverse trajectories, including circular and linear paths, where at least two robots would collide without safety measures. Two examples of these trajectories are shown in Fig. 3. An experiment was considered unsuccessful if the robots collided, or one of the HOCBF-QP problems became infeasible. The success rates for the centralized, decentralized, and relaxed-decentralized filters, using both analytically computed and estimated *Hessian contributions*, are reported in Tab. II.

TABLE II
SUCCESS RATES OF THE HOCBF FILTERING METHODS WITH COMPUTED (COMP.) AND ESTIMATED (EST.) HESSIAN CONTRIBUTION IN THE 4-ROBOT MUJoCo ENVIRONMENT.

Methods	Centralized		Decentralized		Relaxed Decentralized	
	Comp.	Est.	Comp.	Est.	Comp.	Est.
Hessian Contr.						
Success Rate	1.0	1.0	0.875	0.925	0.950	0.950

As shown in Tab. II, the estimated *Hessian contribution* preserved the HOCBF safety guarantees, indicating its reliability when analytical computation is infeasible. While the centralized filters succeeded in all experiments, the decentralized filters failed in some cases due to QP infeasibility. Although relaxation in decentralized filtering mitigated this issue in some experiments, it did not fully eliminate it. Furthermore, approximating the *Hessian contribution* generally helped resolve infeasibility in the decentralized filters by introducing small variations in constraints, but in rare cases, these variations instead led to infeasibility.

B. Experimental Validation on Franka Arms

The proposed algorithms were conducted on two Franka Research 3 arms mounted in proximity of each other, as shown in Fig. 4. Similar to simulation experiments, four ellipsoids per robot were used to define HOCBFs, resulting in a total of 16 HOCBFs. The proposed safety filters, incorporating both analytically computed and estimated *Hessian contributions*, were tested on 10 different intersecting trajectories. Additionally, a collaborative pick-and-place task was designed to illustrate the robots’ ability to collaborate safely under the proposed safety methodology. One such experiment is shown in Fig. 4.

In these experiments, the window length and polynomial order of the Savitzky-Golay filter used to estimate the

Hessian contribution were set to 5 and 2, respectively. The experiments were conducted on a computer equipped with a 24-core Intel Core i9-13900K processor and 64 GB of RAM. All filters, whether based on computed or estimated *Hessian contributions*, successfully executed all experiments while maintaining safety. On average, the filters using analytically computed *Hessian contributions* operated at up to **150 Hz**. Although the Savitzky-Golay filter assumes a constant sampling rate and system interruptions caused variations in the control period beyond the 275 Hz control update rate, the safety filters using estimated *Hessian contributions* could achieve an average operation rate of **400 Hz** without compromising robot safety.

When we conducted the experiments using a less powerful PC with a 16-core Intel Core i7-11700 processor and 64 GB of RAM, analytically computing *Hessian contributions* was infeasible. However, the estimated *Hessian contributions* still operated at **135 Hz** on average. Given that the estimated *Hessian contributions* maintained safety in all the experiments, the proposed estimation method is a valid alternative when high control frequencies are required or when computational constraints prevent analytical computation.

VIII. CONCLUSION

We presented HOCBF-based safety constraints to prevent inter-robotic arm collisions. Using these constraints, we developed centralized, decentralized, and relaxed-decentralized filters. We addressed the computational overhead of HOCBFs by introducing an efficient estimation method based on numerical derivation. We validated the effectiveness of the proposed safety approach through simulation and real-robot experiments. In these experiments, we observed that decentralized filtering can suffer from QP infeasibility in certain scenarios. Although relaxation mitigated this issue, it did not fully resolve it. Future work will focus on addressing this issue and applying the method in more challenging environments, including mobile robots with robotic arms.

REFERENCES

- [1] A. Sathya, P. Sotasakis, R. Van Parys, A. Themelis, G. Pipeleers, and P. Patrinos, "Embedded nonlinear model predictive control for obstacle avoidance using PANOC," in *Proc. European Control Conference*, Limassol, Cyprus, June 2018, pp. 1523–1528.
- [2] X. Zhang, A. Liniger, and F. Borrelli, "Optimization-based collision avoidance," *IEEE Transactions on Control Systems Technology*, vol. 29, no. 3, pp. 972–983, May 2020.
- [3] S. Wei, R. Khorramabakht, P. Krishnamurthy, V. M. Gonçalves, and F. Khorrami, "Collision avoidance for convex primitives via differentiable optimization based high-order control barrier functions," *arXiv preprint arXiv:2410.19159*, 2024.
- [4] L. Wang, A. D. Ames, and M. Egerstedt, "Safety barrier certificates for collisions-free multirobot systems," *IEEE Transactions on Robotics*, vol. 33, no. 3, pp. 661–674, June 2017.
- [5] J. Kim, J. Lee, and A. D. Ames, "Safety-critical coordination of legged robots via layered controllers and forward reachable set based control barrier functions," in *Proc. International Conference on Robotics and Automation*, Yokohama, Japan, May 2024, pp. 3478–3484.
- [6] V. M. Gonçalves, D. Chaikalis, A. Tzes, and F. Khorrami, "Safe multi-agent drone control using control barrier functions and acceleration fields," *Robotics and Autonomous Systems*, vol. 172, p. 104601, February 2024.
- [7] M. Cavorsi, L. Sabattini, and S. Gil, "Multi-robot adversarial resilience using control barrier functions," *IEEE Transactions on Robotics*, vol. 40, pp. 797–815, December 2024.
- [8] P. Mestres, C. Nieto-Granda, and J. Cortés, "Distributed safe navigation of multi-agent systems using control barrier function-based controllers," *IEEE Robotics and Automation Letters*, vol. 9, no. 7, pp. 6760–6767, July 2024.
- [9] C. Smith, Y. Karayiannidis, L. Nalpantidis, X. Gratal, P. Qi, D. V. Dimarogonas, and D. Kragic, "Dual arm manipulation—a survey," *Robotics and Autonomous Systems*, vol. 60, no. 10, pp. 1340–1353, October 2012.
- [10] L. Yan, T. Stouraitis, and S. Vijayakumar, "Decentralized ability-aware adaptive control for multi-robot collaborative manipulation," *IEEE Robotics and Automation Letters*, vol. 6, no. 2, pp. 2311–2318, April 2021.
- [11] A. D. Ames, S. Coogan, M. Egerstedt, G. Notomista, K. Sreenath, and P. Tabuada, "Control barrier functions: Theory and applications," in *Proc. European Control Conference*, Naples, Italy, June 2019, pp. 3420–3431.
- [12] X. Tan, W. S. Cortez, and D. V. Dimarogonas, "High-order barrier functions: Robustness, safety, and performance-critical control," *IEEE Trans. on Automatic Control*, vol. 67, no. 6, pp. 3021–3028, June 2021.
- [13] W. Xiao and C. Belta, "High-order control barrier functions," *IEEE Transactions on Automatic Control*, vol. 67, no. 7, pp. 3655–3662, July 2022.
- [14] V. M. Gonçalves, P. Krishnamurthy, A. Tzes, and F. Khorrami, "Control barrier functions with circulation inequalities," *IEEE Transactions on Control Systems Technology*, vol. 32, no. 4, pp. 1426–1441, 2024.
- [15] K. Shi, J. Chang, S. Feng, Y. Fan, Z. Wei, and G. Hu, "Safe human dual-robot interaction based on control barrier functions and cooperation functions," *IEEE Robotics and Automation Letters*, vol. 9, no. 11, pp. 9581–9588, November 2024.
- [16] K. Shi, J. Liu, J. Chang, and G. Hu, "Distributed quadratic programming for safe human multirobot interaction under task constraints," *IEEE/ASME Transactions on Mechatronics*, pp. 1–13, January 2025.
- [17] C.-C. Wong, S.-Y. Chien, H.-M. Feng, and H. Aoyama, "Motion planning for dual-arm robot based on soft actor-critic," *IEEE Access*, vol. 9, pp. 26 871–26 885, February 2021.
- [18] A. Y. Afaghani and Y. Aiyama, "On-line collision detection of n-robot industrial manipulators using advanced collision map," in *Proc. International Conference on Advanced Robotics*, Istanbul, Turkey, July 2015, pp. 422–427.
- [19] N. Gafur, G. Kanagalingam, A. Wagner, and M. Ruskowski, "Dynamic collision and deadlock avoidance for multiple robotic manipulators," *IEEE Access*, vol. 10, pp. 55 766–55 781, May 2022.
- [20] C. Chang, M. J. Chung, and B. H. Lee, "Collision avoidance of two general robot manipulators by minimum delay time," *IEEE Transactions on Systems, Man, and Cybernetics*, vol. 24, no. 3, pp. 517–522, March 1994.
- [21] C.-H. Chen, L. Chi-Kuang, and F.-I. Chou, "Multiobjective optimization of collaborative robotic task sequence assignment problems under collision-free constraints," *Advances in Mechanical Engineering*, vol. 16, no. 9, p. 16878132241282010, 2024.
- [22] S. Wei, B. Dai, R. Khorramabakht, P. Krishnamurthy, and F. Khorrami, "DiffOcclusion: Differentiable optimization based control barrier functions for occlusion-free visual servoing," *IEEE Robotics and Automation Letters*, vol. 9, no. 4, pp. 3235–3242, April 2024.
- [23] B. Siciliano, L. Sciacivico, L. Villani, and G. Oriolo, *Robotics: Modelling, Planning and Control*. Springer London, 2008.
- [24] E. Rimon and S. P. Boyd, "Obstacle collision detection using best ellipsoid fit," *Journal of Intelligent and Robotic Systems*, vol. 18, pp. 105–126, February 1997.
- [25] H. K. Khalil, *Nonlinear Systems*. Englewood Cliffs, NJ, USA: Prentice-Hall, 1996, vol. 3.
- [26] E. Todorov, T. Erez, and Y. Tassa, "MuJoCo: A physics engine for model-based control," in *Proc. International Conference on Intelligent Robots and Systems*, Vilamoura-Algarve, Portugal, October 2012, pp. 5026–5033.
- [27] A. Savitzky and M. J. Golay, "Smoothing and differentiation of data by simplified least squares procedures," *Analytical Chemistry*, vol. 36, no. 8, pp. 1627–1639, July 1964.
- [28] B. Stellato, G. Banjac, P. Goulart, A. Bemporad, and S. Boyd, "OSQP: an operator splitting solver for quadratic programs," *Mathematical Programming Computation*, vol. 12, no. 4, pp. 637–672, February 2020.